

# Improved RDWIA Physics Models for MCEEP

*An Internal Report to the E00-102 Collaboration*

J. L. Herraiz, J. M. Udías, J. R. Vignote  
Universidad Complutense de Madrid  
E-28040 Madrid  
Spain

joaquin@nuclear.fis.ucm.es  
jose@nuc2.fis.ucm.es  
javier@nuc5.fis.ucm.es<sup>\*</sup>



Kevin Fissum  
Lund University  
SE-221 00 Lund  
Sweden  
kevin.fissum@nuclear.lu.se



**LUNDS**  
UNIVERSITET

---

<sup>\*</sup> present address: Laboratoire de Physique Subatomique et de Cosmologie, F-38026  
Grenoble, France

## Contents

1	Introduction and goals	3
2	Some background information	4
2.1	E89-003 – looking backwards	4
2.2	E00-102 – looking forwards	4
3	Getting started	5
4	The hypercube approach	6
4.1	Overview	6
4.2	RDWIA	7
5	E89-003 revisited	8
5.1	Experiment setup parameters	8
5.2	Simulation results	10
6	Summary and conclusions	21
	Acknowledgement	22
	References	23
	Appendices	26

## 1 Introduction and goals

A general problem invariably encountered during the analysis of  $(e, e'p)$  data is how to correctly address spectrometer acceptances. Experiments are generally performed with spectrometers having significant angular and momentum acceptances. Calculations are generally performed assuming central values for the spectrometer acceptances. Thus, in order to correctly compare data to theory, the acceptance issue must first be put to rest. Two obvious approaches exist – calculations may be averaged over acceptance (requires very well-understood acceptances, time consuming), or acceptance effects may be removed from data via stringent cuts (statistics suffer).

MCEEP [1] is the de-facto Hall A simulation package developed by Paul Ulmer<sup>2</sup>. Via MCEEP, Hall A projects have access to well-developed software models of the High-Resolution Spectrometers (to name just a small subset of that which the toolkit delivers – see below). Unfortunately, in order to keep computation times reasonable, overly simplistic models of the  $(e, e'p)$  interaction are necessarily employed. In order to take MCEEP to the next level, the physics models available to the user must be improved.

Rather than using a single spectral function calculated for a particular “catch-all” kinematics to represent an entire experiment, we have successfully incorporated the RDWIA structure-function calculations of the Madrid Group on an event-by-event basis via fast interpolation on a pre-calculated multidimensional grid which covered an entire experimental acceptance. The payoff is twofold – first, the spectra generated using MCEEP have the most realistic physics possible as their source (which should permit the toolkit to be used to perform much improved data analyses); and second, focused studies of the effects of acceptance averaging on the results will now be possible.

In undertaking this exercise, our short-term goal is to create the ultimate MCEEP model of Jefferson Lab Hall A experiment E00-102: *Testing the Limits of the Single-Particle Model in  $^{16}\text{O}(e, e'p)$*  [2]. We anticipate that the improved physics models will aid dramatically in the analysis of data obtained during the experiment. Our long-term goal is to create the ultimate MCEEP model of Jefferson Lab Hall A experiment E06-007: *Impulse Approximation Limitations to the  $(e, e'p)$  reaction on  $^{208}\text{Pb}$ , identifying Correlations and Relativistic Effects in the Nuclear Medium* [3]. As a first step towards attaining these goals, we have performed an in-depth study of the data obtained in Jefferson Lab Hall A experiment E89-003: *A Study of the Quasielastic  $(e, e'p)$  Reaction in  $^{16}\text{O}$  at High Recoil Momenta* using our newly created toolkit. In this document, we report the results.

---

<sup>2</sup> ulmer@jlab.org

## 2 Some background information

### 2.1 E89-003 – looking backwards

E89-003<sup>3</sup> was the inaugural experiment performed in Hall A at Jefferson Lab. The investigation involved performing absolute cross-section, asymmetry, and structure-function measurements for the  $^{16}\text{O}(e, e'p)$  reaction for  $-350 < p_{\text{miss}} < 350$  MeV/ $c$  and  $0 < E_{\text{miss}} < 120$  MeV in quasielastic (QE) kinematics. It ran during the summer of 1997. As such, much of the experimental equipment used in the measurement was not fully calibrated or commissioned, and many of the data analysis tools were not yet completely developed. One such data analysis tool was MCEEP. At the time of the E89-003 data analysis, multi-foil target models, spectrometer models, energyloss, multiple scattering, and radiative corrections (to name a few) were not available.

It was thus decided to analyze a restricted subset of the data whose behaviour was very well understood. It was determined that events passing into the central acceptance region of the spectrometers were the best behaved. Accordingly, in the resulting data analysis, the spectrometer acceptances were cut very restrictively in the variables  $\theta_{\text{target}}$  (the out-of-plane angle),  $\phi_{\text{target}}$  (the in-plane angle), and  $\delta$  (the deviation from the spectrometer central momentum) – see Table 3. Using data from so-called “white-spectra” measurements, it was shown that when these restrictive cuts were applied, the above-stated variable distributions became “flat” over their cut range. That is, measured spectra could be simulated precisely using a standard random-number generator. Thus, by randomly populating “physics” spectra via simulation, we were able to determine our experimental phase-space for this much-reduced acceptance. As a result, we were able to absolutely analyze the reduced-acceptance subset of the E89-003 data early in the evolution of Hall A. Ultimately, we compared our data to theories based upon the assumption that the acceptance-reducing cuts made the spectrometers approximately “pinhole”; that is, no acceptance averaging of the calculations was performed.

### 2.2 E00-102 – looking forwards

E00-102<sup>4</sup> was the second-generation  $^{16}\text{O}(e, e'p)$  experiment performed in Hall A at Jefferson Lab. The experiment was conceived based upon the insights gained from E89-003. The investigation involved performing absolute cross-section, asymmetry, and structure-function measurements for the  $^{16}\text{O}(e, e'p)$

---

<sup>3</sup> For further information regarding E89-003, see Refs. [4–9].

<sup>4</sup> For further information regarding E00-102, see Refs. [2,10].

reaction for  $-515 < p_{\text{miss}} < 725$  MeV/ $c$  and  $0 < E_{\text{miss}} < 350$  MeV in QE kinematics. It ran in the fall of 2001.

As previously mentioned, MCEEP has truly evolved into a dynamic toolkit for analyzing data obtained in Hall A at Jefferson Lab. All of the previously missing effects – multi-foil target models, spectrometer models, energyloss, multiple scattering, and radiative corrections are presently addressed. Thus, while an analysis similar to that performed for E89-003 is certainly instructive as to the quality of the data we have obtained (see Ref. [10] for an overview), we speculate that it probably no longer does justice to the data. Given the new toolkit, we believe that we no longer will find ourselves restricted to analyzing only the data obtained from the central acceptance region of the spectrometers. We also hope that we will be able to better compare to theory by acceptance-averaging calculations.

We leave testing these speculations to the future. In this work, we focus upon implementing improved RDWIA physics models within MCEEP, and testing the implementation against data.

### 3 Getting started

In order to get started, the following steps were performed:

- version 3.9 (v3.9) of the Monte-Carlo package MCEEP was downloaded and installed on a Hewlett-Packard NX6110 with a CENTRINO processor running Fedora Core 5 [11].
- the  $1p_{1/2}$ -state input decks used by Fissum in 2001 with legacy version 3.5 (v3.5) to setup E00-102 were copied to the above platform. Certain of the kinematics<sup>5</sup> were rerun blindly using the v3.5 input decks and the v3.9 source just to see what happened. Surprisingly large differences between the outputs generated using the two versions existed and were thus investigated. In the end, once the same proton form-factor model was used in both versions of the code<sup>6</sup>, the simulations agreed very well (see Fig. 1).

---

<sup>5</sup> see Appendix A for a sample input deck.

<sup>6</sup> In v3.5, in a comment dated 14-MAR-2000 in the file `/mceep/sources/formfact.f`, it is stated that for the “DIPOLE” form-factor model,  $G_{E_p}$  results from a fit to the Hall A form-factor ratio extracted in E93-027, and that  $G_{M_p}$  is the standard dipole form factor scaled by  $\mu_p$ . In v3.9, in a comment dated 20-SEP-2001 in the file `/mceep/sources/formfact.f`, it is stated that the “DIPOLE” form-factor model corresponds to something entirely different, and that to invoke the same proton form-factor model as in v3.5 (the one detailed above), one must invoke the “HALLA1” form-factor model.

We thus concluded that we had no processor/compiler/platform issues.

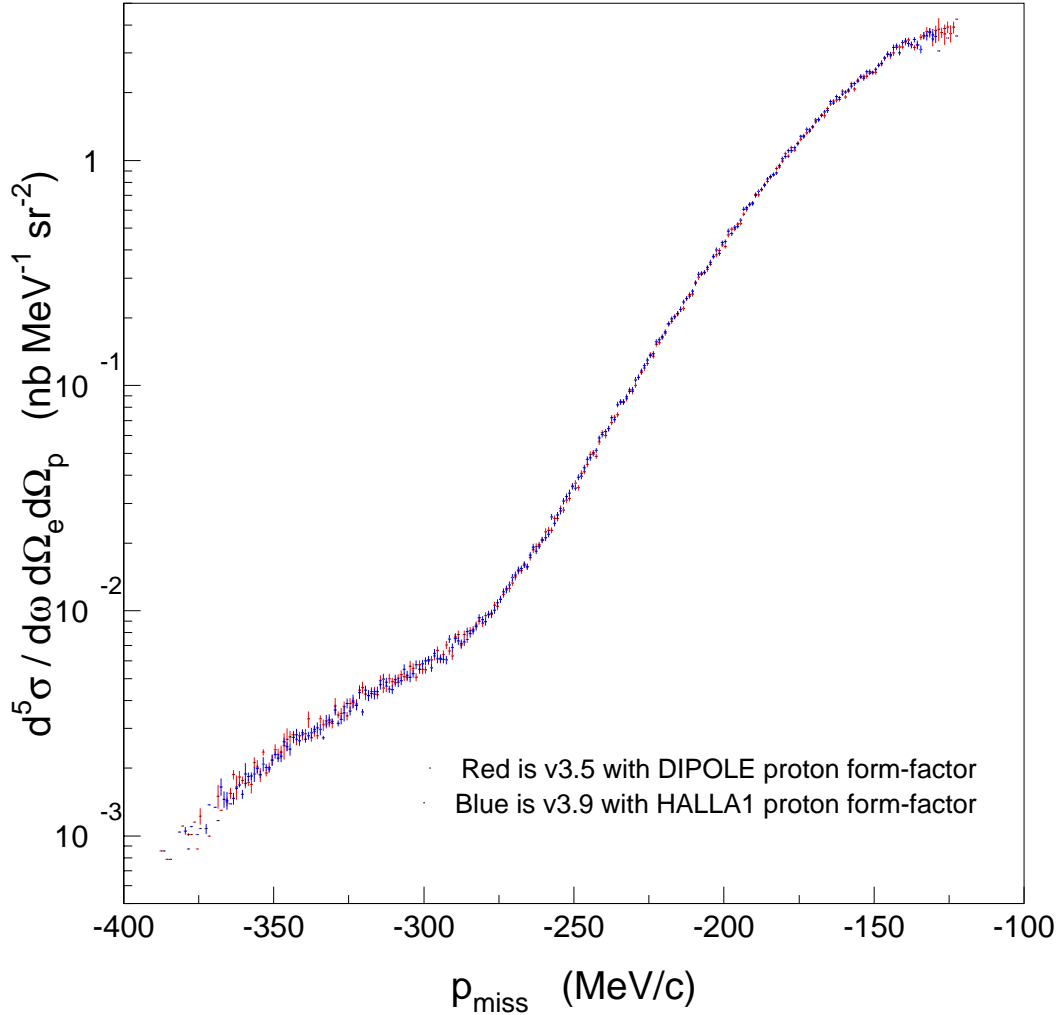


Fig. 1. A comparison between the cross-section output for proton knockout from the  $1p_{1/2}$ -state of  $^{16}\text{O}$  using v3.5 and v3.9 of MCEEP generated using the same input (see Appendix A for a copy of the input deck). The “DIPOLE” form-factor model in v3.5 corresponds to the “HALLA1” form-factor model in v3.9. See text for further details.

## 4 The hypercube approach

### 4.1 Overview

In the past, MCEEP has used hard-coded momentum distributions supplied by the user to describe nucleon-knockout processes. End-user momentum dis-

tributions can be added to the code in a painless fashion. While this is a very efficient approach in terms of processing time and certainly sufficient for setting up experiments (determining rate estimates for example), it is not sufficient for precision studies of experimental data or the effects of extended spectrometer acceptances. This is because in an extended-acceptance experiment, each event can correspond to somewhat different kinematics. Thus, every experimental bin corresponds in principle to a slightly different experiment. By dramatically improving the manner by which the RDWIA calculations are incorporated into MCEEP, we have addressed the issue. To be specific, we “pre-calculate” a structure-function grid (our “hypercube”) which spans the experimental phase space, and then interpolate on this hypercube on an event-by-event basis, extracting the cross section<sup>7</sup>. These cross-section values may then be cut or binned according to the wishes of the user, allowing for detailed studies of the effects of extended acceptances upon the results.

## 4.2 RDWIA

The RDWIA code of the MADRID group has been used to generate the fundamental structure functions  $R_L$ ,  $R_T$ ,  $R_{TL}$ , and  $R_{TT}$  for the  $^{16}\text{O}(e, e'p)$  reaction. The structure functions are then combined to produce the cross section.

To be very specific ( $\hbar = c = 1$ ):

$$\frac{d^5\sigma}{d\Omega_e d\Omega_p d\omega} = K \sigma_{\text{Mott}} [v_L R_L + v_T R_T + v_{TL} R_{TL} \cos(\phi) + v_{TT} R_{TT} \cos(2\phi)], \quad (1)$$

where

$$K = R \frac{p_p E_p}{(2\pi)^3} \quad (\text{phase space factor}), \quad (2)$$

$$R = \left| 1 + \frac{E_p}{E_{\text{recoil}}} \frac{\mathbf{p}_p \cdot \mathbf{p}_{\text{miss}}}{\mathbf{p}_p \cdot \mathbf{p}_p} \right|^{-1} \quad (\text{recoil factor}), \quad (3)$$

$$\sigma_{\text{Mott}} = \left[ \frac{\alpha \cos(\theta_e/2)}{2E_{\text{beam}} \sin^2(\theta_e/2)} \right]^2, \quad (4)$$

and

---

<sup>7</sup> The “rate” option in MCEEP works just as well, allowing the generation of spectra based on the best possible physics input.

$$v_L = \left[ \frac{Q^2}{\mathbf{q}^2} \right]^2, \quad (5)$$

$$v_T = \frac{1}{2} \left[ \frac{Q^2}{\mathbf{q}^2} \right] + \tan^2(\theta_e/2), \quad (6)$$

$$v_{TL} = \left[ \frac{Q^2}{\mathbf{q}^2} \right] \sqrt{\frac{Q^2}{\mathbf{q}^2} + \tan^2(\theta_e/2)}, \quad (7)$$

$$v_{TT} = \frac{1}{2} \left[ \frac{Q^2}{\mathbf{q}^2} \right], \quad (8)$$

are kinematical factors. Variables include  $\phi$  (the angle-of-inclination between the scattering plane and the ejectile plane),  $\mathbf{p}_p$  (the momentum of the knocked-out proton),  $E_p$  (the energy of the knocked-out proton),  $\theta_e$  (the electron-scattering angle),  $\mathbf{p}_{\text{miss}} = \mathbf{p}_p - \mathbf{q} = -\mathbf{p}_{\text{recoil}}$  (the missing momentum),  $E_{\text{beam}}$  (the electron-beam energy),  $Q^2 = q^2 - \omega^2$  (the 4-momentum transfer),  $\mathbf{q}$  (the 3-momentum transfer), and  $\omega$  (the energy transfer)<sup>8</sup>.

The cross section is obviously a function of many variables. In principle, each of these variables may be varied over their experimental ranges in as small a stepsize as desired in order to create as realistic a hypercube as desired. Many variables and a small stepsize simply results in a multi-dimensional space which takes longer to interpolate in order to extract the exact value of the cross section based on the exact kinematics in question.

## 5 E89-003 revisited

As previously mentioned, E89-003 was the inaugural  $^{16}\text{O}(e, e'p)$  experiment performed in Hall A at Jefferson Lab. In this Section, we present an overview of our recreation of E89-003 using vastly improved RDWIA physics models based on the E89-003 results. We then carefully examine the aforementioned extended-acceptance issues using the results of our simulations as compared to the E89-003 data.

### 5.1 Experiment setup parameters

The information presented in Table 1 was used to reconstruct the  $E_{\text{beam}} = 2.442$  GeV  $1p_{1/2}$ -state portion of E89-003.

<sup>8</sup> See also the MCEEP manual and Ref. [9] for further details. The actual coding of the grid and creation of the interface to MCEEP was performed by Vignote together with S. Strauch (see Refs. [12,13]).

Variable	Value
$E_{\text{beam}}$	2.442 GeV
$E_{\text{scattered}}$	1.997 GeV
$p_{\text{cent}}(\text{HRS}_e)$	2.000 GeV/ $c$
$\theta_e$	23.395°
$q$	1.000 GeV/ $c$
$\theta_q$	52.453°
$\omega$	0.445 GeV
$Q^2$	0.802 (GeV/ $c$ ) <sup>2</sup>
$p_{\text{cent}}(\text{HRS}_h)$	0.973 GeV/ $c$
nominal $\theta_{pq}$	$\pm 20.0^\circ, \pm 16.0^\circ, \pm 8.0^\circ, \pm 2.5^\circ, 0^\circ$

Table 1

Setup parameters for E89-003. Recall that QE kinematics were employed, and that the central momentum of the  $\text{HRS}_h$  was purposely set to 0.973 GeV/ $c$  in order to increase the high- $E_{\text{miss}}$  coincidence acceptance available to the spectrometers. “nominal  $\theta_{pq}$ ” refers to the floor angle of the  $\text{HRS}_h$ .

We determined that it was sufficient to generate a set of responses for an (ample) grid in the variables  $\theta_{pq}$ ,  $q$ , and  $\omega$ <sup>9</sup>. This allowed for a much simpler hypercube to be constructed. In order to create a hypercube corresponding to E89-003, we varied the parameters as presented in Table 2.

Variable	Minimum	Maximum	number of steps
$q$	925 MeV/ $c$	1075 MeV/ $c$	15
$\omega$	390 MeV	460 MeV	15
$\theta_{pq}$	-26.0°	+26.0°	75

Table 2

The “input” used to create the RDWIA hypercube representing E89-003. On our modest platform, time to create said hypercube was 22 minutes, and the resulting size is a very manageable 2.5 Mb. In order to perform a MCEEP simulation of 1 M events, 12 seconds are required. This is in fact less time than it takes to perform the conversion of the MCEEP NTUPLE to .hbook format.

In order to replicate the E89-003 data analysis, the cuts detailed in Table 3

<sup>9</sup> There will of course be variations in the other variables; however, we feel that in the interest of efficiency, it is better to deal with them outside the confines of the hypercube. For example, variations in  $\phi$  may easily be “tacked onto” responses, while variations in  $E_{\text{beam}}$  and  $\theta_e$  are easily included via  $\sigma_{\text{Mott}}$ .

have been applied to the simulations.

HRS <sub>e</sub>	HRS <sub>h</sub>
$-50 \text{ mrad} < \theta_{\text{target}} < 45 \text{ mrad}$	$-50 \text{ mrad} < \theta_{\text{target}} < 50 \text{ rad}$
$-26 \text{ mrad} < \phi_{\text{target}} < 24 \text{ mrad}$	$-22 \text{ mrad} < \phi_{\text{target}} < 22 \text{ rad}$
$-3.7\% < \delta < 3.3\%$	$-3.7\% < \delta < 3.3\%$

Table 3

Central water foil cuts employed in the E89-003 data analysis. These cuts have been applied to the results of all simulations discussed in this report.

As the acceptance cuts are very restrictive, the spectrometer options were not considered. Further, we restricted our analysis to the central water foil, and ignored radiative effects, multiple scattering, and energyloss.

## 5.2 Simulation results

In this Section, we present and discuss selected results. After all the simulations were performed, the results were sorted into uniform  $5 \times 5 \times 30$  grid of  $(\omega, q, p_{\text{miss}})$  bins for all kinematics. The bin widths (15 MeV in  $\omega$ , 25 MeV/ $c$  in  $q$ , 5 MeV/ $c$  in  $p_{\text{miss}}$ ) are very similar to those employed in the E89-003 analysis. As was also the case in E89-003, unless otherwise stated, we considered only bins whose phase-space population was better than 50% of the maximum phase-space population.

### 5.2.1 Cross section

All of the E89-003 data (closed black boxes) presented in this Section may be found tabulated in Appendix B.1. Together with the black curves which are the point-acceptance RDWIA calculations from the MADRID Group, they have been taken from Refs. [7,9]. All of the simulated cross-section information may be found tabulated in Appendix C.1.

In Fig. 2, we present the simulated differential cross-section for the removal of  $1p_{1/2}$ -state protons from  $^{16}\text{O}$  in E89-003 kinematics. In the upper three-panel subfigure, hadron spectrometer angles of  $\theta_{pq} = \pm 8.0^\circ, 20.0^\circ$  are shown. In the lower three-panel subfigure, hadron spectrometer angles of  $\theta_{pq} = \pm 2.5^\circ, 16.0^\circ$  are shown. Open red boxes result from our simulations. Each box represents a particular  $(\omega, q, p_{\text{miss}})$  bin.

Consider either subfigure. In the top panel, we show the results of our simulations for the E89-003 acceptances considered in the data analysis. The blue

circles represent the weighted average of the cross-section values over all of the red  $(\omega, q, p_{\text{miss}})$  bins corresponding to a given kinematics. It is clear that the average cross section agrees well with the published data<sup>10</sup>. In the middle panel, we show the  $p_{\text{miss}}$  evolution of the results corresponding to the central  $(\omega, q)$  bin. In the bottom panel, we show the  $p_{\text{miss}}$  evolution of the results corresponding to “extremely reduced” spectrometer acceptances. The cuts used to create these extremely reduced acceptance results included  $\pm 0.1$  mrad in both  $\theta_{\text{target}}$  and  $\phi_{\text{target}}$ , and  $\pm 0.1\%$  in  $\delta$  for both spectrometers. Clearly, as the acceptances are reduced, the simulated results collapse to the point-acceptance RDWIA calculations.

The lack of overlap between the results from the extremely reduced acceptance simulations and the E89-003 data in Fig. 2 may be easily explained. The E89-003 data were plotted in a single bin located at

$$\langle p_{\text{miss}} \rangle = \frac{1}{N} \sum_{i=1}^N p_{\text{miss}}^i, \quad (9)$$

where  $i$  ranged over the total number  $N$  of events which passed the both the cuts applied during the data analysis and the occupancy restriction on the phase-space volume. The extremely reduced acceptance results have (as expected) a kinematically predicted  $p_{\text{miss}}$  (acceptance plays absolutely no role). These acceptance effects are in general larger for lower  $\theta_{pq}$ , but cannot be completely dismissed at large  $\theta_{pq}$  – see again the  $\langle p_{\text{miss}} \rangle = 330$  MeV/ $c$  data point whose extremely reduced acceptance value and full-acceptance values lie well-separated from each other.

In Fig. 3, we present the simulated differential cross section for the removal of  $1p_{1/2}$ -state protons from  $^{16}\text{O}$  as a function of  $p_{\text{miss}}$  in E89-003 kinematics for extreme  $\text{HRS}_h$  angles. Each panel shows a different  $\theta_{pq}$ , either  $\pm 2.5^\circ$  or  $\pm 20.0^\circ$ . The red contours resulted from the E89-003 cuts previously discussed. The black boxes resulted from “reduced” acceptance cuts:  $\pm 1.0$  mrad in  $\theta_{\text{target}}$ ,  $\pm 0.5$  mrad in  $\phi_{\text{target}}$ , and  $\pm 1.0\%$  in  $\delta$ . It is clear from these plots that the previously observed effect of the extended-acceptance upon  $\langle p_{\text{miss}} \rangle$  is largest upon the  $\theta_{pq} \pm 2.5^\circ$  data; that is, the reduced-acceptance distributions do not correspond to the “average” of the full-acceptance distributions<sup>11</sup>.

<sup>10</sup> Except of course for  $\langle p_{\text{miss}} \rangle = 330$  MeV/ $c$ . We have been completely unable to simulate this data point. We attribute the difference to either a cut in the data analysis of which we are completely unaware, or contributions from events originating in either the upstream or downstream water foils (which we have not considered). We have decided not to spend any more time chasing this, but rather to focus our efforts upon the E00-102 data.

<sup>11</sup> That said, we stress that the  $\theta_{pq} \pm 2.5^\circ$  data are amongst the most complicated data to analyze given the fact that  $\text{H}(e, e'p)$  is well within the experimental acceptance. There have been cuts employed to remove such events for these kinematics

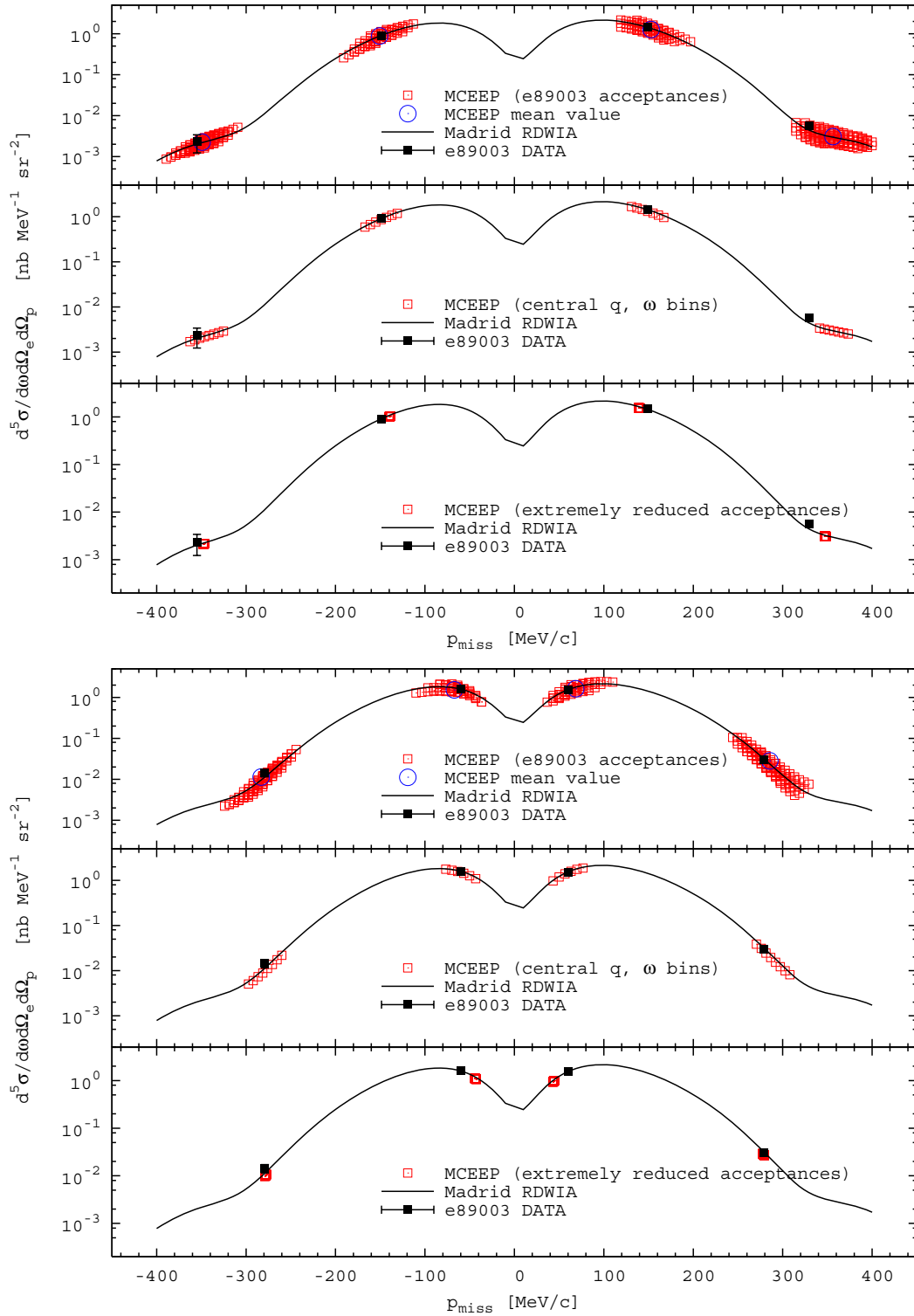


Fig. 2. Differential cross section for the removal of  $1p_{1/2}$ -state protons from  $^{16}\text{O}$  as a function of  $p_{\text{miss}}$  in E89-003 kinematics. In the upper subfigure, hadron spectrometer angles of  $\theta_{pq} = \pm 8.0^\circ$  and  $20.0^\circ$  are shown. In the lower subfigure, hadron spectrometer angles of  $\theta_{pq} = \pm 2.5^\circ$  and  $16.0^\circ$  are shown. See text for further details.

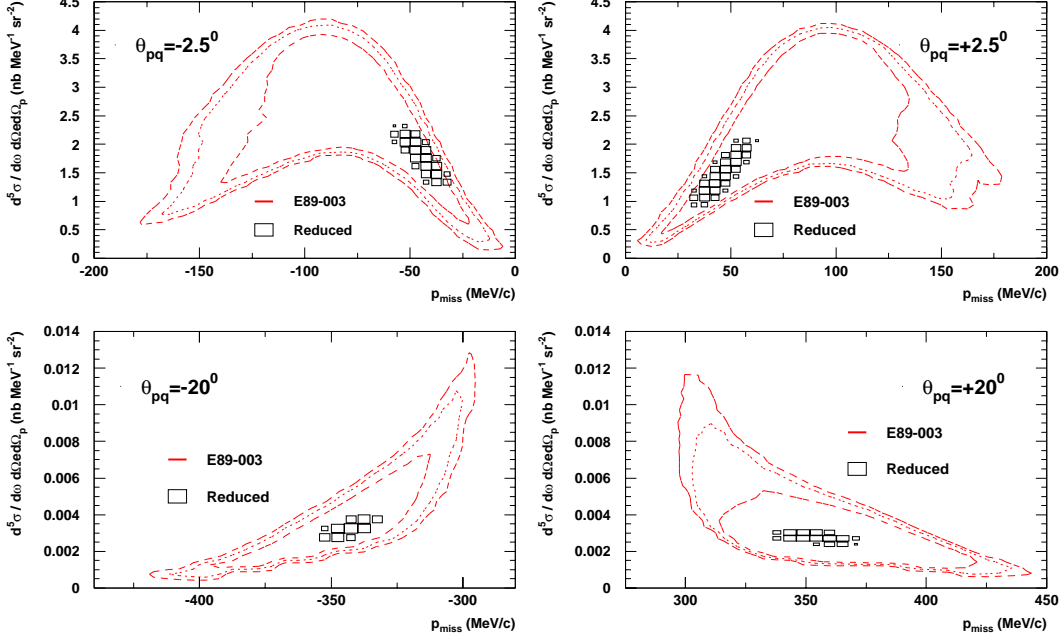


Fig. 3. Simulated differential cross section for the removal of  $1p_{1/2}$ -state protons from  $^{16}\text{O}$  as a function of  $p_{\text{miss}}$  in E89-003 kinematics. Each panel shows a different  $\theta_{pq}$ , either  $\pm 2.5^\circ$  or  $\pm 20.0^\circ$ . See text for further details.

### 5.2.2 Transverse-longitudinal asymmetry $A_{TL}$

All of the E89-003 data (closed black boxes) presented in this Section may be found tabulated in Appendix B.2. Together with the black curves which are the point-acceptance RDWIA calculations from the MADRID Group, they have been taken from Refs. [7,9]. All of the simulated  $A_{TL}$  information may be found tabulated in Appendix C.2.

The transverse-longitudinal asymmetry  $A_{TL}$  is given by

$$A_{TL} = \frac{\sigma(\phi = 0^\circ) - \sigma(\phi = 180^\circ)}{\sigma(\phi = 0^\circ) + \sigma(\phi = 180^\circ)}. \quad (10)$$

$A_{TL}$  is a particularly valuable quantity as it is systematically more precise than a structure function measurement or even an absolute cross section. However, evaluation of  $A_{TL}$  requires careful consideration of the experimental phase space on either side of  $\mathbf{q}$ , and is thus sensitive “pairwise” to acceptance issues.

---

that we have not included. Again, we have decided not to spend any more time chasing this, but rather to focus our efforts upon the E00-102 data.

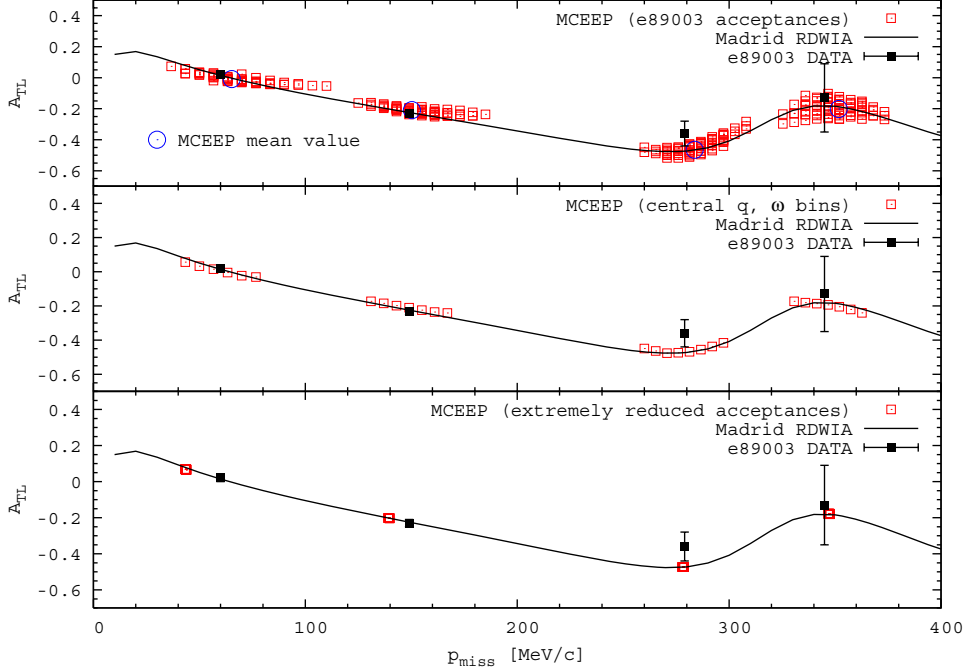


Fig. 4. Transverse-longitudinal asymmetry  $A_{TL}$  for the removal of  $1p_{1/2}$ -state protons from  $^{16}\text{O}$  in E89-003 kinematics. A phase-space volume occupancy of 50% of the maximum occupancy is required simultaneously on either side of  $\mathbf{q}$ . See text for further details.

In Fig. 4, we present the simulated transverse-longitudinal asymmetry  $A_{TL}$  for the removal of  $1p_{1/2}$ -state protons from  $^{16}\text{O}$  in E89-003 kinematics. All of the previously discussed analysis cuts presented in Table 3 have been applied. Open red boxes result from our simulations, and each box represents a particular  $(\omega, q, p_{\text{miss}})$  bin.

In the top panel, we show the results of our simulations for the E89-003 acceptances considered in the data analysis. The blue circles represent the average of the  $A_{TL}$  values over all of the red  $(\omega, q, p_{\text{miss}})$  bins corresponding to a given kinematics. It is clear that the averaged simulated  $A_{TL}$  values agree reasonably well with the published data<sup>12</sup>. In the middle panel, we show the  $p_{\text{miss}}$  evolution of the results corresponding to the central  $(\omega, q)$  bin. In the bottom panel, we show the  $p_{\text{miss}}$  evolution of the results corresponding to “extremely reduced” spectrometer acceptances. The cuts used to create these extremely reduced acceptance results are as before:  $\pm 0.1$  mrad in both  $\theta_{\text{target}}$  and  $\phi_{\text{target}}$ , and  $\pm 0.1\%$  in  $\delta$  for both spectrometers. As in the case of the cross-section results, as the acceptances are reduced, the simulated results collapse to the

<sup>12</sup> Again, we speculate the difference between the data and the present simulation is due to the upstream and downstream water foils which subtend different kinematics than the central foil does. We have chosen not to consider this effect in this work, preferring to pay closer attention to it in our simulations for E00-102.

point-acceptance RDWIA calculations.

Fig. 4 clearly demonstrates that extended acceptances do have an effect on the data. As in the case of the cross section, we again see that the E89-003 data do not lie where the extremely reduced acceptance simulations predict they should. Further, we note that the relative positioning of the  $A_{TL}$  data and the extremely reduced acceptance  $A_{TL}$  simulated data is different from the relative positioning of the simulated cross-section values and cross-section data.

Is this behaviour a function of the restrictions on the phase-space volume occupancy? In Fig. 5, we again present the simulated transverse-longitudinal asymmetry  $A_{TL}$  for the removal of  $1p_{1/2}$ -state protons from  $^{16}\text{O}$  in E89-003 kinematics. All of the previously discussed cuts have been applied and all of the previously detailed definitions hold; however, we do not make any requirement on the level of simultaneous phase-space volume occupancy<sup>13</sup>.

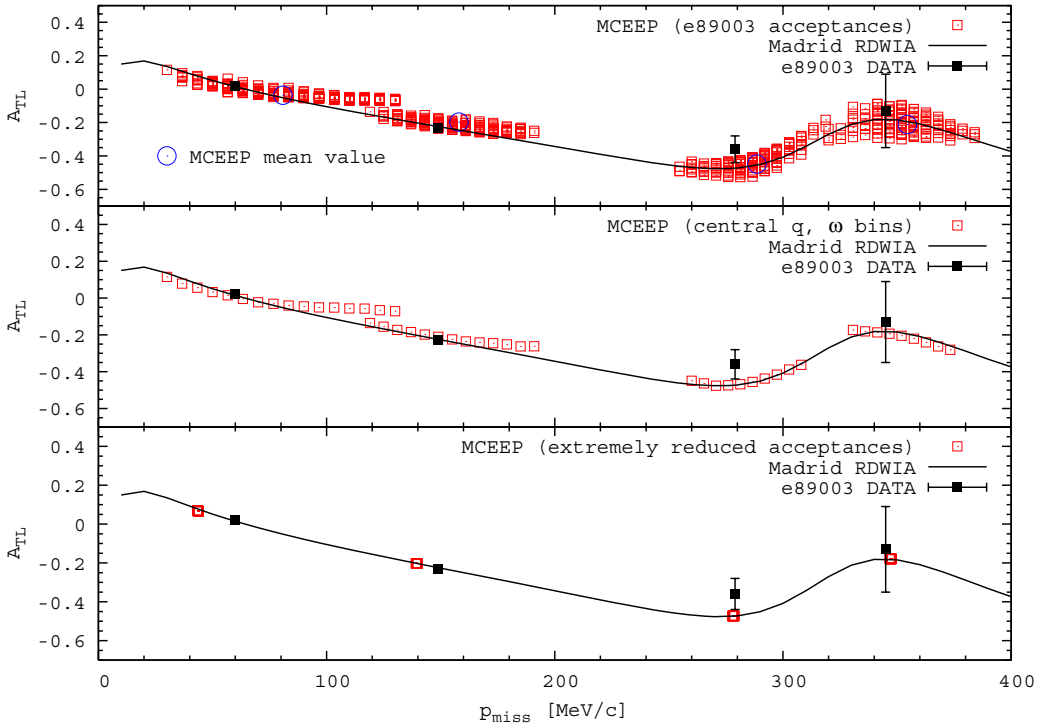


Fig. 5. Transverse-longitudinal asymmetry  $A_{TL}$  for the removal of  $1p_{1/2}$ -state protons from  $^{16}\text{O}$  in E89-003 kinematics. “No” requirement has been made upon the simultaneous phase-space volume occupancy. See text for further details.

We can see that ignoring the simultaneous 50% population restriction on the

<sup>13</sup> Of course, we do require that corresponding bins on either side of  $\mathbf{q}$  are occupied; that is, at least one event in each of the pairwise bins.

phase-space volume dramatically increases the effect the extended acceptances have on the data by looking at the blue circles in the top panel. These circles represent the average of the  $A_{TL}$  values over all of the red  $(\omega, q, p_{\text{miss}})$  bins corresponding to a given kinematics. While it is clear that the averaged simulated  $A_{TL}$  values no longer agree with the published data, we stress that they should not – we are now averaging over a substantially different “data” set.

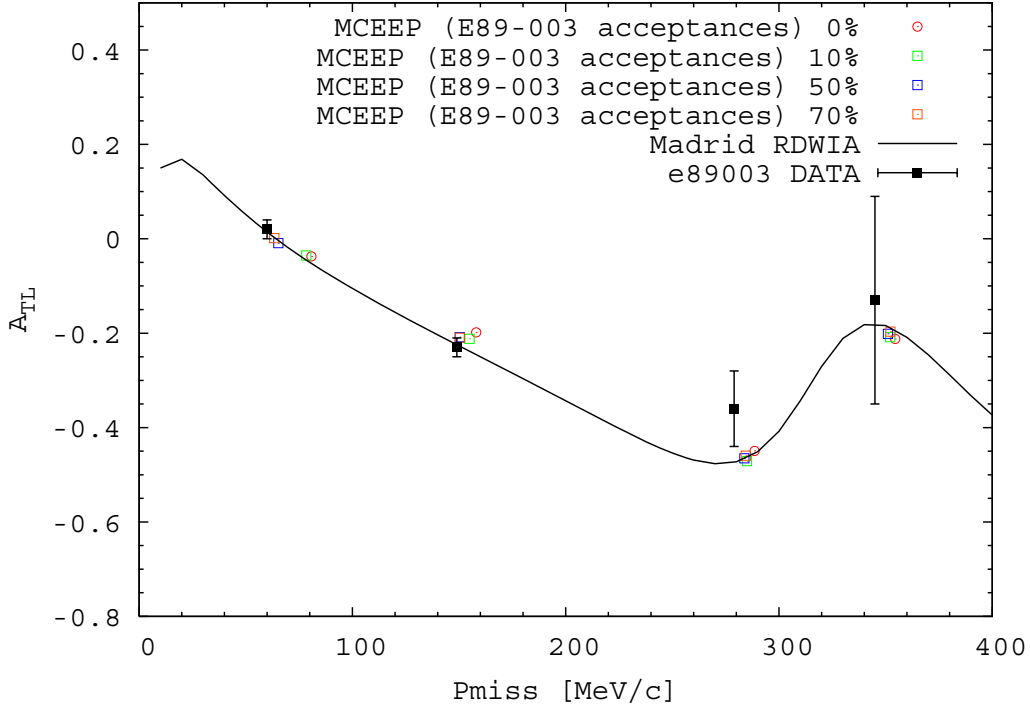


Fig. 6. Transverse-longitudinal asymmetry  $A_{TL}$  for the removal of  $1p_{1/2}$ -state protons from  $^{16}\text{O}$  in E89-003 kinematics for four increasingly severe requirements on the pairwise simultaneous phase-space volume occupancies. For the  $\theta_{pq} = \pm 2.5^\circ$  data, an effect that is much more dramatic than that demonstrated by the data from the other spectrometer angles is clearly observed. See text for further details.

As more acceptance essentially means more data and greater statistical precision in the measurement, we have studied the effect of varying the severity of the required simultaneous phase-space volume population. In Fig. 6, we present the simulated transverse-longitudinal asymmetry  $A_{TL}$  for the removal of  $1p_{1/2}$ -state protons from  $^{16}\text{O}$  in E89-003 kinematics for four increasingly severe requirements on the simultaneous phase-space volume occupancies – 0% (open red circles)<sup>14</sup>, 10% (open green boxes), 50% (open blue boxes) and 70% (open orange boxes). All of the analysis cuts summarized in Table 3 have been

<sup>14</sup> Again, we stress that by 0%, we mean we only require corresponding bins on either side of  $\mathbf{q}$  to be pairwise simultaneously populated. A single event is enough.

applied. Each box (circle) represents a weighted average over all the available  $(\omega, q, p_{\text{miss}})$  bins.

We see little effect due to relaxing the requirement on the phase-space volume for  $\theta_{pq} = \pm 8.0^\circ$ ,  $\theta_{pq} = \pm 16.0^\circ$ , and  $\theta_{pq} = \pm 20.0^\circ$ . The simulations sit more or less on the calculation. Agreement is especially good at high  $p_{\text{miss}}$  for  $\theta_{pq} = \pm 16.0^\circ$ , and  $\theta_{pq} = \pm 20.0^\circ$ . A “converging to the calculation” effect appears at  $\theta_{pq} = \pm 8.0^\circ$  as the severity of the requirement is increased. And for the  $\theta_{pq} = \pm 2.5^\circ$  simulations, a very clear effect may be observed – as the requirement is relaxed,  $\langle p_{\text{miss}} \rangle$  increases. That said, the data follow the calculation very well for all levels of simultaneous population at this low  $p_{\text{miss}}$ .

### 5.2.3 Transverse-longitudinal interference $R_{TL}$

All of the E89-003 data (closed black boxes) presented in this Section may be found tabulated in Appendix B.3. Together with the black curves which are the point-acceptance RDWIA calculations from the MADRID Group, they have been taken from Refs. [7,9]. All of the simulated  $R_{TL}$  information may be found tabulated in Appendix C.3.

The transverse-longitudinal interference  $R_{TL}$  is given by

$$R_{TL} = \frac{1}{2v_{TL}K\sigma_{\text{Mott}}} [\sigma(\phi = 0^\circ) - \sigma(\phi = 180^\circ)] \quad (11)$$

The quantity  $R_{TL}$  is more difficult to extract correctly from data than either  $\sigma$  or  $A_{TL}$ . The evaluation of  $R_{TL}$  requires correct absolute normalization of two cross sections, together with careful consideration of the experimental phase space on either side of  $\mathbf{q}$ . It is a quantity that is thus also sensitive “pairwise” to acceptance issues.

Note that internal self-consistency checks have been performed successfully on  $R_{TL}$ . Recall that we create a given cross section from four point-source RDWIA structure functions according to Eqn. 1. One of the four structure functions is of course  $R_{TL}$ . Using such cross sections together with Eqn. 11, we determine the transverse-longitudinal interference  $R_{TL}$  over the entire experimental acceptance. We find that when we extremely reduce the experimental acceptance to  $\pm 0.1$  mrad in both  $\theta_{\text{target}}$  and  $\phi_{\text{target}}$ , and  $\pm 0.1\%$  in  $\delta$  for both spectrometers, we recover to better than 5% the point-source value for  $R_{TL}$ . This internal self-closure after a very complicated journey through our simulation is very reassuring.

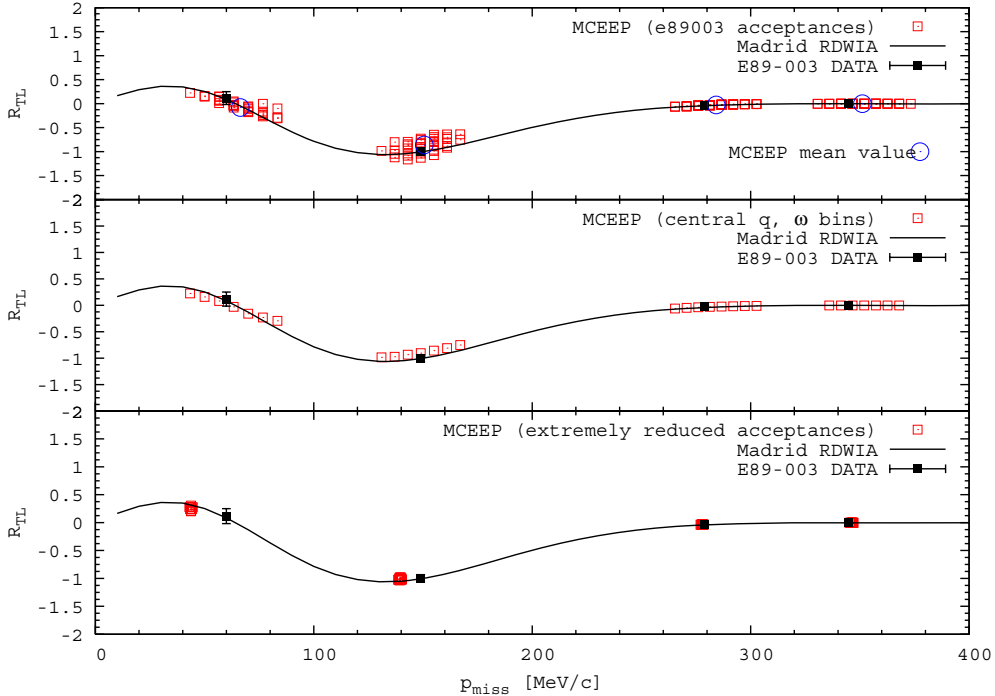


Fig. 7. Transverse-longitudinal interference  $R_{TL}$  for the removal of  $1p_{1/2}$ -state protons from  $^{16}\text{O}$  in E89-003 kinematics. A phase-space volume occupancy of 50% of the maximum occupancy is required simultaneously on either side of  $\mathbf{q}$ . See text for further details.

In Fig. 7, we present the simulated transverse-longitudinal interference  $R_{TL}$  for the removal of  $1p_{1/2}$ -state protons from  $^{16}\text{O}$  in E89-003 kinematics. All of the previously discussed analysis cuts presented in Table 3 have been applied. Open red boxes result from our simulations, and each box represents a particular  $(\omega, q, p_{\text{miss}})$  bin.

In the top panel, we show the results of our simulations for the E89-003 acceptances considered in the data analysis. The blue circles represent the average of the  $R_{TL}$  values over all of the red  $(\omega, q, p_{\text{miss}})$  bins corresponding to a given kinematics. It is clear that the averaged simulated  $R_{TL}$  values agree reasonably well with the published data<sup>15</sup>. In the middle panel, we show the  $p_{\text{miss}}$  evolution of the results corresponding to the central  $(\omega, q)$  bin. In the bottom panel, we show the  $p_{\text{miss}}$  evolution of the results corresponding to “extremely reduced” spectrometer acceptances. The cuts used to create these extremely reduced acceptance results are as before:  $\pm 0.1$  mrad in both  $\theta_{\text{target}}$  and  $\phi_{\text{target}}$ , and  $\pm 0.1\%$  in  $\delta$  for both spectrometers. As in the case of the cross-section and

<sup>15</sup> Recall from our discussion of the asymmetry  $A_{TL}$  that the upstream and downstream water foils which subtend different kinematics than the central foil does. We do not consider this effect in this work, preferring to pay closer attention to it in our simulations for E00-102.

asymmetry  $A_{TL}$  results, as the acceptances are reduced, the simulated results collapse to the point-acceptance RDWIA calculations.

Fig. 7 clearly demonstrates that extended acceptances do have an effect on the data. As in the case of the cross section and the asymmetry  $A_{TL}$ , we again see that the E89-003 data do not lie where the extremely reduced acceptance simulations predict they should. This time, however, the relative positioning of the interference  $R_{TL}$  data and the extremely reduced acceptance  $R_{TL}$  simulated data is very similar to the relative positioning of the simulated asymmetry  $A_{TL}$  values and data.

We again investigate whether or not this behaviour is a function of the restrictions on the phase-space volume occupancy. In Fig. 8, we again present the simulated transverse-longitudinal interference  $R_{TL}$  for the removal of  $1p_{1/2}$ -state protons from  $^{16}\text{O}$  in E89-003 kinematics. All of the previously discussed cuts have been applied and all of the previously detailed definitions hold, but we do not make any requirement on the level of simultaneous phase-space volume occupancy<sup>16</sup>.

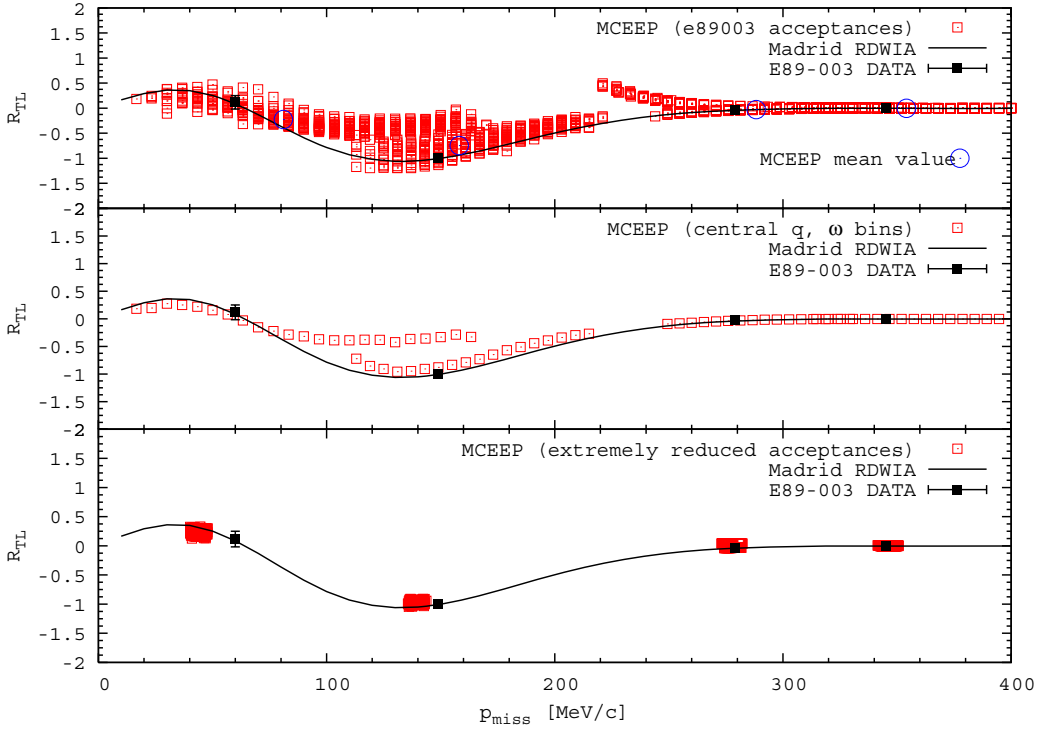


Fig. 8. Transverse-longitudinal interference  $R_{TL}$  for the removal of  $1p_{1/2}$ -state protons from  $^{16}\text{O}$  in E89-003 kinematics. “No” requirement has been made upon the simultaneous phase-space volume occupancy. See text for further details.

<sup>16</sup> Again, corresponding bins on either side of  $\mathbf{q}$  must be occupied; that is, at least one event in each of the pairwise bins.

We can again see that ignoring the simultaneous 50% population restriction on the phase-space volume dramatically increases the effect the extended acceptances have on the data by looking at the blue circles in the top panel. These circles represent the average of the  $R_{TL}$  values over all of the red ( $\omega$ ,  $q$ ,  $p_{\text{miss}}$ ) bins corresponding to a given kinematics. As anticipated, the observed effect is much more dramatic in  $R_{TL}$  than in either the cross section or  $A_{TL}$ . Again, while it is clear that the averaged simulated  $R_{TL}$  values no longer agree with the published data, we stress that they should not – we are now averaging over a substantially different “data” set.

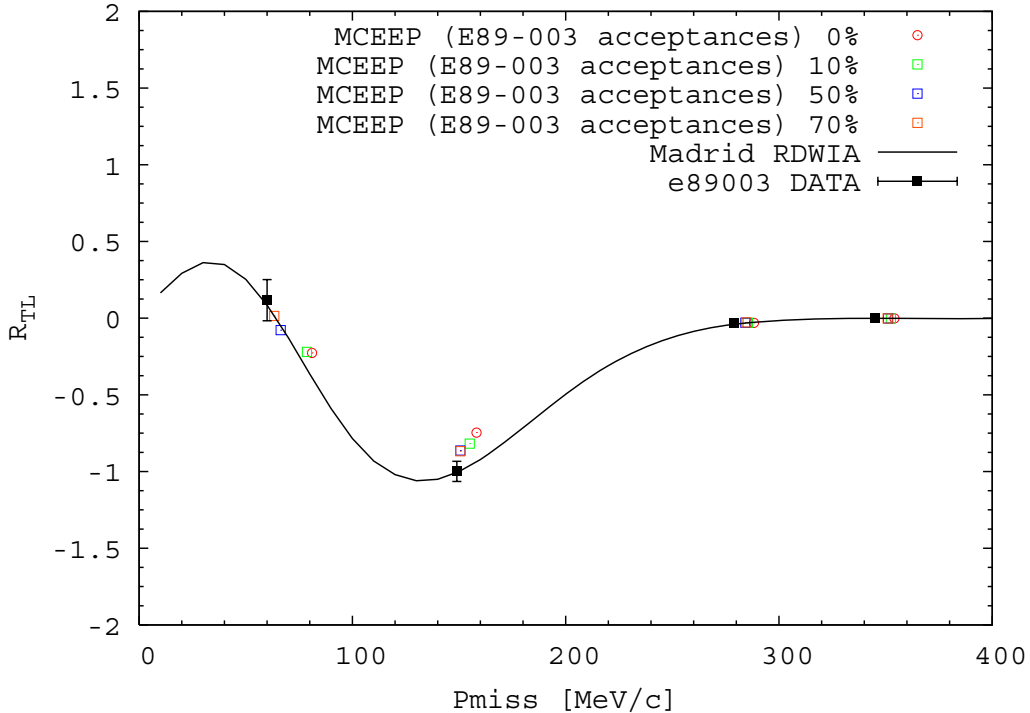


Fig. 9. Transverse-longitudinal interference  $R_{TL}$  for the removal of  $1p_{1/2}$ -state protons from  $^{16}\text{O}$  in E89-003 kinematics for four increasingly severe requirements on the pairwise simultaneous phase-space volume occupancies. For the  $\theta_{pq} = \pm 2.5^\circ$  data, an effect that is much more dramatic than that demonstrated by the data from the other spectrometer angles is clearly observed. See text for further details.

Finally, we have again studied the effect of varying the severity of the required simultaneous phase-space volume population. In Fig. 9, we present the simulated effective transverse-longitudinal interference  $R_{TL}$  for the removal of  $1p_{1/2}$ -state protons from  $^{16}\text{O}$  in E89-003 kinematics for four increasingly severe requirements on the simultaneous phase-space volume occupancies – 0% (open red circles)<sup>17</sup>, 10% (open green boxes), 50% (open blue boxes) and 70%

<sup>17</sup> Recall that by 0%, we mean we only require corresponding bins on either side of  $q$  to be pairwise simultaneously populated. A single event is enough.

(open orange boxes). All of the analysis cuts summarized in Table 3 have been applied. Each box (circle) represents a weighted average over all the available  $(\omega, q, p_{\text{miss}})$  bins.

We see little effect due to relaxing the requirement on the phase-space volume for  $\theta_{pq} = \pm 16.0^\circ$  and  $\theta_{pq} = \pm 20.0^\circ$ . The simulations all sit more or less on the calculation. As observed in our studies of  $A_{TL}$ , a “converging to the calculation” effect again appears as the severity of the requirement is increased, but this time for both  $\theta_{pq} = \pm 2.5^\circ$  and  $\theta_{pq} = \pm 8.0^\circ$ . Also for  $\theta_{pq} = \pm 2.5^\circ$  and  $\theta_{pq} = \pm 8.0^\circ$ , we again see that as the requirement is relaxed,  $\langle p_{\text{miss}} \rangle$  increases. And while the “data” follow the calculation very well for all levels of simultaneous population at  $p_{r\text{miss}} \sim 70 \text{ MeV}/c$ , the overall agreement is poorer at  $p_{r\text{miss}} \sim 150 \text{ MeV}/c$ .

## 6 Summary and conclusions

We have successfully incorporated the RDWIA structure-function calculations of the Madrid Group on an event-by-event basis into a specialized version of MCEEP based upon v3.9. This is done via fast interpolation on a pre-calculated multidimensional grid (hypercube) on an event by event basis. The volume of the hypercube may be easily be set to cover an experimental acceptance.

We have used Jefferson Lab Hall A experiment E89-003: *A Study of the Quasielastic ( $e, e'p$ ) Reaction in  $^{16}\text{O}$  at High Recoil Momenta* as our laboratory for testing our newly created toolkit. We have successfully replicated the cross-section, transverse-longitudinal asymmetry  $A_{TL}$ , and effective interference response-function  $R_{TL}$  results obtained in E89-003 taking into consideration cuts performed in the data analysis and experimental acceptances. We did not consider mult-foil targets, energyloss, or radiative effects.

We are convinced that our code is working “as advertised”. From the results of our investigations, we conclude the following:

- although we were all well aware of this fact before we began this project, we have again demonstrated that experimental acceptances can have a large effect upon extracted results. The acceptances must be treated carefully and correctly or the information extracted from the experiment is meaningless.
- by only considering the central water foil, we knowingly built disagreement between our results and the data into our work. We believe the upstream and downstream water foils will most certainly have an affect on the average value of the data, as they subtend different kinematics. Especially in regions of  $p_{\text{miss}}$  where the cross section is varying violently, these effects can

be large. We decided it was prudent to address these issues in the upcoming E00-102 data analysis, rather than to try unravel them using the legacy data.

- at very low  $p_{\text{miss}}$  where  $H(e, e'p)$  “contamination” of the  $^{16}\text{O}(e, e'p)$  data occurs, a set of cuts more closely resembling that used in the data analysis is required. Again, we decided to investigate these kinematics more carefully in the upcoming E00-102 data analysis, rather than to try unravel them using the legacy data.
- our studies of  $A_{TL}$  for various requirements on the simultaneous population of the  $(\omega, q, p_{\text{miss}})$  bins on either side of  $\mathbf{q}$  indicate that the value of 50% employed in the E89-003 data analysis may not have been optimal. At low  $p_{\text{miss}}$  such as  $\theta_{pq} = \pm 2.5^\circ$ , regardless of the requirement employed, the simulations track with the calculation. At moderate  $p_{\text{miss}}$  such as  $\theta_{pq} = \pm 8.0^\circ$ , a clear convergence effect is observed as the severity of the restriction is increased. Perhaps most importantly, at high  $p_{\text{miss}}$  where the cross section is small, almost no effect is observed.
- our studies of  $R_{TL}$  for various requirements on the simultaneous population of the  $(\omega, q, p_{\text{miss}})$  bins on either side of  $\mathbf{q}$  also indicate that the value of 50% employed in the E89-003 data analysis may not have been optimal. As in the  $A_{TL}$  results, at low  $p_{\text{miss}}$  such as  $\theta_{pq} = \pm 2.5^\circ$ , regardless of the requirement employed, the simulations track with the calculation. At moderate  $p_{\text{miss}}$  such as  $\theta_{pq} = \pm 8.0^\circ$ , a clear convergence effect is observed as the severity of the restriction is increased. And again, perhaps most importantly, at high  $p_{\text{miss}}$  where the cross section is small, almost no effect is observed.

Our results indicate that it may be possible to require a lower level of simultaneous population of the  $(\omega, q, p_{\text{miss}})$  bins on either side of  $\mathbf{q}$  at high  $p_{\text{miss}}$  in our analysis of the E00-102 data. In doing so, we can potentially improve upon our statistics by as much as a factor of two – a significant gain. Conversely, we may be forced to require a higher level of population at lower  $p_{\text{miss}}$ . Happily, we have statistics to burn in this region. We thus must carefully study these effects for E00-102 – stay tuned!

## Acknowledgement

JRV acknowledges the valuable contribution made by S. Strauch to the coding of the grid and creation of the interface to MCEEP, and expresses his gratitude for the fruitful collaboration during time spent at Jefferson Lab and the years since then. As a group, we thank Paul Ulmer for the countless hours he spent over the years creating, upgrading, expanding, testing, troubleshooting, and

documenting MCEEP. Paul has never been too busy to help and has never tired of answering what at times amounted to the same questions over and over (and over...). Thank you, Paul, and good luck!

## References

- [1] [www.physics.odu.edu/~ulmer/mceep/mceep.html](http://www.physics.odu.edu/~ulmer/mceep/mceep.html)
- [2] [www.jlab.org/~fissum/e00102/e00102.html](http://www.jlab.org/~fissum/e00102/e00102.html)
- [3] [hallaweb.jlab.org/collab/PAC/PAC29/PR-06-007-Pb-QuasiElastic.ps](http://hallaweb.jlab.org/collab/PAC/PAC29/PR-06-007-Pb-QuasiElastic.ps)
- [4] [www.jlab.org/~fissum/e89003.html](http://www.jlab.org/~fissum/e89003.html)
- [5] J. Gao, Ph.D. thesis, Massachusetts Institute of Technology, 1999; see also [www.jlab.org/~fissum/e89003/learned/jgaothesis.ps.gz](http://www.jlab.org/~fissum/e89003/learned/jgaothesis.ps.gz)
- [6] N. Liyanage, Ph.D. thesis, Massachusetts Institute of Technology, 1999; see also [www.jlab.org/~fissum/e89003/learned/nliyanagethesis.ps.gz](http://www.jlab.org/~fissum/e89003/learned/nliyanagethesis.ps.gz)
- [7] J. Gao *et al.*, Phys. Rev. Lett. **84**, 3265 (2000).
- [8] N. Liyanage *et al.*, Phys. Rev. Lett. **86**, 5670 (2001).
- [9] K. G. Fissum *et al.*, Phys. Rev. C **70**, 034606 (2004).
- [10] M. Andersson, Licentiat thesis, Lund University, 2005; see also [www.jlab.org/~fissum/e00102/learned/lic/lic\\_a4.pdf](http://www.jlab.org/~fissum/e00102/learned/lic/lic_a4.pdf)
- [11] [fedora.redhat.com](http://fedora.redhat.com)
- [12] S. Dieterich *et al.*, Phys. Lett. **B500**, 47 (2001).
- [13] S. Strauch *et al.*, Phys. Rev. Lett. **91**, 052301 (2002).

## Appendix A Sample v3.5 input deck

```

500000
4,4,4,4,4
938.2796,1,12.1
4620.,0.,0.,4121.,12.5,0.,1066.,-46.83,0.
3.5,-3.5,3.5,-3.5
'R','R',60.,130.,60.,130.
89.07,1.,1.
45.,2.2,2.2
16.,8.,0.8889,1,0
-57.4,3,-0.02707,-0.02373,-0.00167,0.00167,0.02373,0.02707
1.109,1.100
0.8,0.,0.,0.,0.
0.,0.,0.,0.,0.
0.,0.,0.,0.,0.
'R',0.0001,0.0001
'E',T,21,-90.,0.,0.,0.
'NTU',1,0.,'d_minus_p12cent_etgt1.ntu'
'DFT',110.9
'CUT','G','R',-6.09,6.09,1
'CUT','G','R',-3.15,3.15,3
'DFT',8.00
'CUT','G','R',-6.49,6.49,1
'CUT','G','R',-3.34,3.34,3
'DFT',-118.9
'HRS','E',T,T,T,T,T
'NTU',1,45.,'d_minus_p12cent_efp.ntu'
'TOF',23.4
'DFT',-30.0
'RES','K',2,2,4.0D-3
'RES','K',4,2,4.0D-3
'DFT',15.0
'RES','K',2,2,8.2D-4
'RES','K',4,2,8.2D-4
'DFT',15.0
'TRK','hrs_vdc2.par'
'HRI','E'
'NTU',1,0.,'d_minus_p12cent_etgt2.ntu'
'P',T,18,-90.,0.,0.,0.
'DFT',110.0
'CUT','G','R',-6.09,6.09,1
'CUT','G','R',-3.15,3.15,3
'DFT',8.00
'CUT','G','R',-6.49,6.49,1
'CUT','G','R',-3.34,3.34,3
'DFT',-118.0
'HRS','H',T,T,T,T,T

```

# tries  
for default ranges  
m\_eject,z\_eject,em\_bound  
kinematics  
momentum acceptances  
nominal solid angles  
luminosity,time,spec\_fac  
for singles only  
targ: a,z,dens,targ\_mod,eloss\_mod  
targ: cell start/end  
drift to aperture - nom. sld. ang.  
beam: pol, vert, disp, df, tof\_win  
beam: FWHM in cm,cm,mr,mr,%  
beam: offset in cm,cm,mr,mr,%  
beam: raster shape, X size, Y size  
ELECTRON ARM

drift to front face of coll.  
cut on x\_coll  
cut on y\_coll  
drift to back face of coll.  
cut on x\_coll  
cut on y\_coll  
drift back to target  
aperture tests and tgt→fp

ToF marker  
drift to exit window  
mscat in window - theta  
mscat in window - phi  
drift half way to VDC1  
mscat in air - theta  
mscat in air - phi  
drift to VDC1  
VDC reconstruction  
inverse map: fp→tgt

HADRON ARM  
drift to front face of coll.  
cut on x\_coll  
cut on y\_coll  
drift to back face of coll.  
cut on x\_coll  
cut on y\_coll  
drift back to target  
aperture tests and tgt→fp

```

'TOF',23.4
'DFT',-30.0
'RES','K',2,2,4.0D-3
'RES','K',4,2,4.0D-3
'DFT',15.0
'RES','K',2,2,8.2D-4
'RES','K',4,2,8.2D-4
'DFT',15.0
'TRK','hrs_vdc2.par'
'HRI','H'
0
0
2
'NTU',-1,11,4,10,12,15,16,18,22,24,25,26,34,'d_minus_p12cent.cross.ntu'
'NTU',1,11,4,10,12,15,16,18,22,24,25,26,34,'d_minus_p12cent.rate.ntu'
Comments: 16O(e,e'p) p12 with JLAB Hall A HRS
100 uA on waterfall target
energyloss, external radiation excluded
ToF marker
drift to exit window
mscat in window - theta
mscat in window - phi
drift half way to VDC1
mscat in air - theta
mscat in air - phi
drift to VDC1
VDC reconstruction
inverse map: fp→tgt
# global cuts
# specific cuts
# plots

```

## Appendix B E89-003 data

The data quoted in this Appendix are taken from Refs. [7,9].

### B.1 Cross-section data

Cross-section data for QE proton knockout from the  $1p_{1/2}$ -state of  $^{16}\text{O}$  obtained at  $E_{\text{beam}} = 2.442$  GeV are presented in Table 4.

$\theta_{pq}$ ( $^{\circ}$ )	$\langle p_{\text{miss}} \rangle$ (MeV/c)	$d^5\sigma/d\omega d\Omega_e d\Omega_p$ (nb/MeV/sr $^2$ )	(sys) (%)
-20.0	-355.0	$0.0023 \pm 0.0011$	5.5
-16.0	-279.0	$0.0143 \pm 0.0029$	5.7
-8.0	-149.0	$0.9060 \pm 0.0260$	5.5
-2.5	-60.0	$1.5981 \pm 0.0456$	5.4
2.5	60.0	$1.5380 \pm 0.0513$	5.4
8.0	149.0	$1.4605 \pm 0.0261$	5.5
16.0	279.0	$0.0303 \pm 0.0029$	5.7
20.0	330.0	$0.0057 \pm 0.0005$	5.6

Table 4

Measured cross-section data for  $\langle Q^2 \rangle = 0.800$  (GeV/c) $^2$ ,  $\langle \omega \rangle = 436$  MeV, and  $\langle T_p \rangle = 427$  MeV. The  $p_{\text{miss}}$  bins were 20 MeV/c wide.

### B.2 Asymmetries $A_{TL}$

Asymmetries for QE proton knockout from the  $1p_{1/2}$ -state of  $^{16}\text{O}$  obtained at  $E_{\text{beam}} = 2.442$  GeV are presented in Table 5.

$\langle p_{\text{miss}} \rangle$ (MeV/c)	$A_{TL}$	
	(stat)	(sys)
60.0	0.02 ± 0.02	± 0.02
149.0	-0.23 ± 0.02	± 0.03
279.0	-0.36 ± 0.08	± 0.04
345.0	-0.13 ± 0.22	± 0.05

Table 5

The asymmetry  $A_{TL} \langle Q^2 \rangle = 0.800 \text{ (GeV}/c)^2$ ,  $\langle \omega \rangle = 436 \text{ MeV}$ , and  $\langle T_p \rangle = 427 \text{ MeV}$ . The  $p_{\text{miss}}$  bins were 20 MeV/c wide.

### B.3 Effective interference response functions $R_{TL}$

Effective interference response functions for QE proton knockout from the  $1p_{1/2}$ -state of  $^{16}\text{O}$  obtained at  $E_{\text{beam}} = 2.442 \text{ GeV}$  are presented in Table 6.

$\langle p_{\text{miss}} \rangle$ (MeV/c)	$R_{TL} \text{ (fm}^3\text{)}$	
	(stat)	(sys)
60.0	0.117 ± 0.134	± 0.037
149.0	-0.999 ± 0.066	± 0.077
279.0	-0.029 ± 0.007	± 0.002
345.0	-0.002 ± 0.003	± 0.001

Table 6

The effective interference response function  $R_{TL} \langle Q^2 \rangle = 0.800 \text{ (GeV}/c)^2$ ,  $\langle \omega \rangle = 436 \text{ MeV}$ , and  $\langle T_p \rangle = 427 \text{ MeV}$ . The  $p_{\text{miss}}$  bins were 20 MeV/c wide.

## Appendix C Simulation results

### C.1 Cross-section simulations

The simulated cross section for QE proton knockout from the  $1p_{1/2}$ -state of  $^{16}\text{O}$  obtained at  $E_{\text{beam}} = 2.442$  GeV is presented in this Appendix. The cuts discussed in the text on  $\theta_{\text{target}}$ ,  $\phi_{\text{target}}$ , and  $\delta$  have been used in the generation of these results. A normalization factor of 0.7 has been applied.

$\Delta V/V_{\text{max}}$	$\theta_{pq} = -2.5^\circ$				$\theta_{pq} = 2.5^\circ$			
	events		$\langle p_{\text{miss}} \rangle$	$\langle \sigma \rangle$	events		$\langle p_{\text{miss}} \rangle$	$\langle \sigma \rangle$
	bins	(rel)	(MeV/c)	(nb)	bins	(rel)	(MeV/c)	(nb)
0%	750	1.000	-79.6	1.52	750	1.000	80.6	1.63
10%	279	0.918	-77.1	1.54	288	0.920	77.9	1.65
20%	183	0.783	-74.7	1.56	190	0.783	75.2	1.66
30%	129	0.652	-72.1	1.55	129	0.642	72.6	1.65
40%	84	0.502	-68.7	1.54	85	0.498	70.6	1.67
50%	59	0.394	-67.2	1.52	56	0.371	68.5	1.63
60%	41	0.299	-66.9	1.52	42	0.298	69.0	1.64
70%	27	0.211	-68.3	1.51	28	0.212	70.8	1.71
80%	15	0.124	-68.3	1.53	10	0.083	75.1	1.73
90%	2	0.019	-60.0	1.54	3	0.027	61.2	1.19

Table 7

Simulated cross section in nb MeV $^{-1}$  sr $^{-2}$  as a function of  $\langle p_{\text{miss}} \rangle$  in MeV/c for increasing levels of constraint imposed on the phase-space volume for  $\theta_{pq} = \mp 2.5^\circ$ .

$\Delta V/V_{\max}$	$\theta_{pq} = -8.0^\circ$				$\theta_{pq} = 8.0^\circ$			
	events		$\langle p_{\text{miss}} \rangle$	$\langle \sigma \rangle$	events		$\langle p_{\text{miss}} \rangle$	$\langle \sigma \rangle$
	bins	(rel)	(MeV/c)	(nb)	bins	(rel)	(MeV/c)	(nb)
0%	750	1.000	-154.0	0.850	750	1.000	156.8	0.119
10%	246	0.944	-152.7	0.865	255	0.938	155.6	0.122
20%	178	0.846	-152.4	0.869	189	0.846	154.8	0.122
30%	121	0.709	-151.6	0.875	134	0.720	154.3	0.123
40%	92	0.613	-150.3	0.895	93	0.591	153.4	0.125
50%	72	0.527	-150.8	0.881	70	0.495	152.9	0.126
60%	56	0.442	-150.7	0.876	59	0.439	153.4	0.125
70%	45	0.373	-151.5	0.857	45	0.356	154.1	0.122
80%	34	0.293	-152.6	0.844	35	0.287	155.1	0.120
90%	12	0.110	-154.8	0.823	17	0.147	158.7	0.112

Table 8

Simulated cross section in nb MeV<sup>-1</sup> sr<sup>-2</sup> as a function of  $\langle p_{\text{miss}} \rangle$  in MeV/c for increasing levels of constraint imposed on the phase-space volume for  $\theta_{pq} = \mp 8.0^\circ$ .

$\Delta V/V_{\max}$	$\theta_{pq} = -16.0^\circ$				$\theta_{pq} = 16.0^\circ$			
	events		$\langle p_{\text{miss}} \rangle$	$\langle \sigma \rangle$	events		$\langle p_{\text{miss}} \rangle$	$\langle \sigma \rangle$
	bins	(rel)	(MeV/c)	(nb)	bins	(rel)	(MeV/c)	(nb)
0%	750	1.000	-283.2	0.013	750	1.000	289.7	0.027
10%	249	0.965	-282.8	0.013	270	0.967	289.0	0.027
20%	206	0.912	-282.7	0.013	217	0.906	288.3	0.028
30%	160	0.820	-283.2	0.012	176	0.829	287.9	0.027
40%	128	0.731	-283.3	0.011	136	0.724	286.5	0.028
50%	105	0.649	-283.6	0.011	107	0.626	285.6	0.028
60%	83	0.550	-283.3	0.011	88	0.547	285.6	0.027
70%	69	0.477	-283.5	0.011	70	0.458	286.9	0.025
80%	52	0.373	-282.3	0.011	55	0.372	289.1	0.022
90%	26	0.196	-282.4	0.011	25	0.179	296.5	0.015

Table 9

Simulated cross section in nb MeV<sup>-1</sup> sr<sup>-2</sup> as a function of  $\langle p_{\text{miss}} \rangle$  in MeV/c for increasing levels of constraint imposed on the phase-space volume for  $\theta_{pq} = \mp 16.0^\circ$ .

$\Delta V/V_{\max}$	$\theta_{pq} = -20.0^\circ$				$\theta_{pq} = 20.0^\circ$			
	events		$\langle p_{\text{miss}} \rangle$	$\langle \sigma \rangle$	events		$\langle p_{\text{miss}} \rangle$	$\langle \sigma \rangle$
	bins	(rel)	(MeV/c)	(nb)	bins	(rel)	(MeV/c)	(nb)
0%	750	1.000	-348.9	0.002	750	1.000	358.6	0.003
10%	243	0.970	-348.8	0.002	258	0.967	357.9	0.003
20%	208	0.927	-348.2	0.002	216	0.919	357.8	0.003
30%	176	0.865	-348.9	0.002	181	0.852	357.5	0.003
40%	139	0.762	-348.9	0.002	148	0.764	357.6	0.003
50%	107	0.649	-349.2	0.002	115	0.651	356.3	0.003
60%	81	0.537	-349.4	0.002	82	0.513	354.5	0.003
70%	65	0.454	-346.9	0.002	69	0.448	355.0	0.003
80%	48	0.354	-346.8	0.002	45	0.312	360.5	0.003
90%	36	0.271	-347.4	0.002	27	0.194	362.5	0.003

Table 10

Simulated cross section in nb MeV<sup>-1</sup> sr<sup>-2</sup> as a function of  $\langle p_{\text{miss}} \rangle$  in MeV/c for increasing levels of constraint imposed on the phase-space volume for  $\theta_{pq} = \mp 20.0^\circ$ .

### C.2 Asymmetry $A_{TL}$ simulations

The simulated asymmetry  $A_{TL}$  for QE proton knockout from the  $1p_{1/2}$ -state of <sup>16</sup>O obtained at  $E_{\text{beam}} = 2.442$  GeV is presented in this Appendix. The cuts discussed in the text on  $\theta_{\text{target}}$ ,  $\phi_{\text{target}}$ , and  $\delta$  have been used in the generation of these results. Constraints on the phase-space volume have been imposed simultaneously on either side of  $\mathbf{q}$ ; that is, there must be at least one event in each of the pairwise bins to qualify for 0% occupation.

$\Delta V/V_{\max}$	$\theta_{pq}=\pm 2.5^\circ$			
	bins	events (rel)	$\langle p_{\text{miss}} \rangle$ (MeV/c)	$A_{TL}$
0%	467	1.000	81.1	-0.038
10%	228	0.827	78.7	-0.036
20%	134	0.638	75.1	-0.033
30%	90	0.503	72.2	-0.027
40%	57	0.358	69.2	-0.024
50%	32	0.217	66.4	-0.013
60%	18	0.127	63.3	-0.003
70%	5	0.039	63.4	0.002
80%	—	—	—	—
90%	—	—	—	—

Table 11

Simulated asymmetry  $A_{TL}$  as a function of  $\langle p_{\text{miss}} \rangle$  in MeV/c for increasing levels of constraint for  $\theta_{pq} = \pm 2.5^\circ$ .

$\Delta V/V_{\max}$	$\theta_{pq}=\pm 8.0^\circ$			
	bins	events (rel)	$\langle p_{\text{miss}} \rangle$ (MeV/c)	$A_{TL}$
0%	341	1.000	158.1	-0.201
10%	150	0.755	155.0	-0.212
20%	95	0.594	153.0	-0.211
30%	74	0.505	152.1	-0.206
40%	52	0.388	151.2	-0.208
50%	39	0.309	150.6	-0.210
60%	23	0.201	150.0	-0.208
70%	17	0.153	150.6	-0.210
80%	11	0.102	152.8	-0.214
90%	2	0.019	152.0	-0.216

Table 12

Simulated asymmetry  $A_{TL}$  as a function of  $\langle p_{\text{miss}} \rangle$  in MeV/c for increasing levels of constraint for  $\theta_{pq} = \pm 8.0^\circ$ .

$\Delta V/V_{\max}$	$\theta_{pq}=\pm 16.0^\circ$			
	bins	events (rel)	$\langle p_{\text{miss}} \rangle$ (MeV/c)	$A_{TL}$
0%	269	1.000	288.3	-0.461
10%	122	0.735	285.4	-0.458
20%	90	0.621	284.6	-0.462
30%	70	0.527	284.5	-0.459
40%	53	0.431	284.4	-0.465
50%	41	0.356	284.3	-0.463
60%	28	0.267	283.9	-0.455
70%	22	0.215	284.8	-0.457
80%	12	0.122	285.8	-0.458
90%	3	0.031	290.2	-0.427

Table 13

Simulated asymmetry  $A_{TL}$  as a function of  $\langle p_{\text{miss}} \rangle$  in MeV/c for increasing levels of constraint for  $\theta_{pq} = \pm 16.0^\circ$ .

$\Delta V/V_{\max}$	$\theta_{pq}=\pm 20.0^\circ$			
	bins	events (rel)	$\langle p_{\text{miss}} \rangle$ (MeV/c)	$A_{TL}$
0%	241	1.000	354.1	-0.218
10%	114	0.727	352.5	-0.208
20%	86	0.631	351.3	-0.206
30%	67	0.533	352.3	-0.202
40%	53	0.455	351.7	-0.202
50%	43	0.390	351.2	-0.201
60%	29	0.289	351.9	-0.197
70%	23	0.236	351.0	-0.192
80%	14	0.149	352.7	-0.197
90%	6	0.065	348.5	-0.200

Table 14

Simulated asymmetry  $A_{TL}$  as a function of  $\langle p_{\text{miss}} \rangle$  in MeV/c for increasing levels of constraint for  $\theta_{pq} = \pm 20.0^\circ$ .

C.2 Effective interference response function  $R_{TL}$  simulations

The simulated effective interference response function  $R_{TL}$  for QE proton knockout from the  $1p_{1/2}$ -state of  $^{16}\text{O}$  obtained at  $E_{\text{beam}} = 2.442$  GeV is presented in this Appendix. The cuts discussed in the text on  $\theta_{\text{target}}$ ,  $\phi_{\text{target}}$ , and  $\delta$  have been used in the generation of these results. Constraints on the phase-space volume have been imposed simultaneously on either side of  $\mathbf{q}$ ; that is, there must be at least one event in each of the pairwise bins to qualify for 0% occupation.

$\Delta V/V_{\text{max}}$	$\theta_{pq} = \pm 2.5^\circ$			
	bins	events (rel)	$\langle p_{\text{miss}} \rangle$ (MeV/c)	$R_{TL}$
0%	467	1.000	81.1	-0.227
10%	228	0.827	78.7	-0.220
20%	134	0.638	75.1	-0.206
30%	90	0.502	72.2	-0.169
40%	57	0.358	69.2	-0.149
50%	32	0.217	66.4	-0.078
60%	18	0.127	63.3	-0.016
70%	5	0.039	63.4	0.014
80%	—	—	—	—
90%	—	—	—	—

Table 15

Simulated effective transverse-longitudinal interference response function  $R_{TL}$  as a function of  $\langle p_{\text{miss}} \rangle$  in MeV/c for increasing levels of constraint for  $\theta_{pq} = \pm 2.5^\circ$ .

$\Delta V/V_{\max}$	$\theta_{pq} = \pm 8.0^\circ$			
	bins	events (rel)	$\langle p_{\text{miss}} \rangle$ (MeV/c)	$R_{TL}$
0%	341	1.000	158.1	-0.745
10%	150	0.755	155.0	-0.819
20%	95	0.594	153.0	-0.838
30%	74	0.505	152.1	-0.828
40%	52	0.388	151.2	-0.846
50%	39	0.309	150.6	-0.863
60%	23	0.201	150.0	-0.862
70%	17	0.153	150.6	-0.868
80%	11	0.102	152.8	-0.839
90%	2	0.019	152.0	-0.859

Table 16

Simulated effective transverse-longitudinal interference response function  $R_{TL}$  as a function of  $\langle p_{\text{miss}} \rangle$  in MeV/c for increasing levels of constraint for  $\theta_{pq} = \pm 8.0^\circ$ .

$\Delta V/V_{\max}$	$\theta_{pq} = \pm 16.0^\circ$			
	bins	events (rel)	$\langle p_{\text{miss}} \rangle$ (MeV/c)	$R_{TL}$
0%	269	1.000	288.3	-0.030
10%	122	0.735	285.4	-0.030
20%	90	0.621	284.6	-0.031
30%	70	0.527	284.5	-0.030
40%	53	0.431	284.4	-0.030
50%	41	0.356	284.3	-0.029
60%	28	0.267	283.9	-0.028
70%	22	0.215	284.8	-0.027
80%	12	0.122	285.8	-0.026
90%	3	0.031	290.2	-0.018

Table 17

Simulated effective transverse-longitudinal interference response function  $R_{TL}$  as a function of  $\langle p_{\text{miss}} \rangle$  in MeV/c for increasing levels of constraint for  $\theta_{pq} = \pm 16.0^\circ$ .

$\Delta V/V_{\max}$	$\theta_{pq} = \pm 20.0^\circ$			
	bins	events (rel)	$\langle p_{\text{miss}} \rangle$ (MeV/c)	$R_{TL}$
0%	241	1.000	354.1	-0.002
10%	114	0.727	352.5	-0.208
20%	86	0.631	351.3	-0.206
30%	67	0.533	352.3	-0.202
40%	53	0.455	351.7	-0.202
50%	43	0.390	351.2	-0.201
60%	29	0.289	351.9	-0.197
70%	23	0.236	351.0	-0.192
80%	14	0.149	352.7	-0.197
90%	6	0.065	348.5	-0.200

Table 18

Simulated effective transverse-longitudinal interference response function  $R_{TL}$  as a function of  $\langle p_{\text{miss}} \rangle$  in MeV/c for increasing levels of constraint for  $\theta_{pq} = \pm 20.0^\circ$ .